PCCP

Accepted Manuscript

ROYAL SOCIETY OF CHEMISTRY

www.rsc.org/pccp

Structural morphologies of high-pressure polymorphs of strontium hydrides

Yanchao Wang[1], Hui Wang[1,2+], John S. Tse[1,2,3*], Toshiaki Iitaka[4], and Yanming Ma[1,3]

[1]State Key Laboratory of Superhard Materials, Jilin University, Changchun 130012, China

[2]Department of Physics and Engineering Physics, University of Saskatchewan, Saskatoon, Saskatchewan, S7N 5B2, Canada.

[3]Beijing Computational Science Research Center, Beijing 10084, China.

[4]Computational Astrophysics Laboratory, RIKEN, 2-1 Hirosawa, Wako, Saitama 351-0198, Japan.

[+]huiwang@jlu.edu.cn, [*]John.Tse@usask.ca

Abstract

It is now known that the structure and property of a material can be significantly altered under extreme compression. In this work, structural search was performed to investigate the phase stabilities and structures of SrH_{2n} (n = 1–5) in the pressure range 50–300 GPa. The high-pressure polymorphs reveal a variety of hydrogen structural units ranging from monatomic hydride to linear and bent H_3 and spiral polymer chains. A novel graphene like H-layer structure was found to exist in SrH_{10} at 300 GPa. The structural diversity in the predicted high pressure structures provides an opportunity for an in-depth analysis of the chemical bonding in the high pressure polyhydrides. It is shown from theoretical calculations that electronegativity of molecular hydrogen is similar to group 13 and 14 elements. This resulted in electrons being transferred from Sr to the hydrogen molecules. Thus, a consideration of the number of valence electrons available from Sr that can be shared among the H_2, serves as a useful guide to rationalize the structures of the H-moieties. An alternative description of the high pressure structures differs from a previous study is presented here.

Introduction

Pressure is a versatile thermodynamic parameter to modify the structure of a material. Elemental solids can show myriad novel structural types with changing pressure[1, 2]. Even simple elements, such as the alkali metals, can assume complex structures with unexpected properties[2-5]. Recently reported examples include the observation of insulator phases in Li[6] and Na[7]. At times, the complex structures observed seem to defy a systematic and logical explanation[8]. Theoretical investigations have shown that many of the structures and structural transformations can be rationalized by consideration of the orbital re-hybridization induced in a confined environment[2]. In ref. 1, an excellent overview of the chemical bonding at high pressure was presented. The most significant finding is the universal behaviour of electron transfer from the atomic valence region to open interstitial sites, in some case, which leads to the formation of localized electrides, a high-pressure analogue of the Wigner crystal[2, 9]. In an orbital description, localization of electrons in a non-atom site can be viewed as the result of overlaps from spatially extended higher angular momentum orbitals of neighboring atoms, such as the 2*p* orbital in Li[10] and the 5*d* in Cs[2]. In fact, a 6*s*–5*d* transition in Cs was already proposed in 1950[11]. It was found that, due to the confinement potential under external compression, the orbital energy of Cs 5*d* became *lower* than that of the 6*s* orbital. The tendency of valence electron transfer has important consequences for the nature of chemical bonding and the crystal structure. This phenomenon is manifested in the unanticipated observation of the formation of K–Ag binary alloys at high pressure[12]. A similar concept is applied in this work to elucidate the investigation the structure hydrogen units in the predicted high-pressure crystal structures of strontium hydrides (SrH_{2n}, n = 1–5).

Recent research on the synthesis of hydrogen-rich binary metallic alloys at high pressure was stimulated by the proposal that these dense hydrogen alloys are potential superconductors with high critical temperatures, T_c[13]. Indeed, very recently, a very high T_c of 190 K has been observed in hydrogen sulphide (H_2S) compressed to 200 GPa[14]. In the course on the search of potential superconducting dense hydrogen alloys, new efficient structural search and optimization techniques, such as the evolution algorithms[15], particle-swarm optimization[16] and structures constructed randomly[17] were developed and have greatly facilitated theoretical investigations[18]. As a result, a large number of metal hydrides have been studied. Depending on the composition of the alloy and the pressure, many group I (Li[19], K[20], Rb[21], and Cs[22]) and group II (Mg[23], Ca[24], Sr[25] and Ba[26]) elements alloyed with H_2 at high pressure have been found to display a large

variety of structural types and chemical bonding. A notable result is the prediction of a superconducting phase of CaH_6 that formed from a sodalite framework of H atoms with Ca encapsulated in the cavities[24]. To further explore the diversity of metal–H_2 interactions, this work reports the analysis of the structure and chemical bonding in the lowest enthalpy polymorphs of strontium hydride (SrH_{2n}, n = 1–5) from 50 to 300 GPa. Unique among the group I and II hydrides, a large variety of H units was predicted to exist in SrH_{2n}[25]. In a previous study on the same subject, the structure and structural changes in high pressure Sr hydrides have been attributed to the dominance of planar H…H hexagonal layer patterns and weak interactions between them leading to the formation of the cage-like structures[25]. Here, we report two new structural morphologies of high-pressure polymorphs of strontium hydrides and offer a different perspective on the structural description. In particular, it is demonstrated that the hydrogen molecule is a good electron acceptor. From quantitative analysis of the charge densities, considerable charge transfers from Sr to the hydrogen were found. A systematic describe of the structure of the H-species in the crystals can therefore be explained by characters of charge transfers.

Computational Details

Our structure prediction is based on a global minimum search of the enthalpy surfaces obtained by *ab initio* calculations at a constant pressure, through CALYPSO (crystal structure analysis by particle swarm optimization) methodology and its same-name code[16, 27], which is free for academic use, by registering at *http:www.calypso.cn*. The *ab initio* calculations were performed using density functional theory within the Perdew-Burke-Ernzerhof (PBE) parameterization[28] of the generalized gradient approximation as implemented in the Vienna ab initio simulation package (VASP) code[29]. The all-electron projector-augmented wave (PAW) method[30] was adopted with $4s^2 4p^6 5s^2$ and $1s^1$ as valence electrons for Sr and H atoms, respectively. Plane-wave energy cutoffs of 500 eV and 700 eV, and uniform Monkhorst-Pack (MP) meshes[31] for Brillouin zone (BZ) sampling with resolutions of $2\pi\times0.06$ Å^{-1} and $2\pi\times0.03$ Å^{-1} were employed in the structure predictions and subsequent calculations (e.g. of thermodynamic stability), respectively. This usually gave well-converged total energies (within ~ 1 meV per atom). The phonon calculations were carried out by a finite displacement approach[32] through the PHONOPY code[33]. The 2x2x3 supercells containing 252 atoms were used in the phonon

calculations of $P\bar{3}$, $P321$ and $R\bar{3}m$ structures of SrH_6. A 2x2x2 supercell containing 88 atoms was used in the phonon calculation of $R\bar{3}m$ structure of SrH_{10}. The crystal structures were plotted by VESTA software[34].

Results and discussion

The lowest-enthalpy structures, relative to Sr metal and solid H_2, for various SrH_{2n} stoichiometries found at different pressures are depicted in Fig. 1A. Most of the predicted structures reported here have already been identified in the earlier study[25] with the exception of a new SrH_6 structure found at 250 GPa and a novel graphene like H-layered structure, similar to the proposed phase-IV of solid hydrogen[35, 36], that has not been reported for SrH_{10}. A summary of the predicted most stable high pressure phases from 0 to 300 GPa are shown in Fig. 1B. Before embarking on detail analysis, a survey of the distinctive features observed in the predicted structures (Fig. 1C) is given below.

The stable high pressure polymorphs of SrH_2 are all consisted solely of monatomic H (hydride). The orthorhombic structure observed experimentally under ambient pressure is reproduced correctly. At 50 GPa, the most stable SrH_2 structure has a hexagonal $P6_3/mmc$ space group. For SrH_4, two different moieties: H_2 and monatomic H were found in both predicted lowest enthalpy crystal structures at 50 and 150 GPa. More diversify H structural units are found in SrH_6: at 50 and 150 GPa, $C2/c$ and $P\bar{3}$ structure structures are formed from monatomic H, H_2 and Sr atoms. Further compression to 200 GPa resulted in bent H_3 units with a $P321$ space group. This is a new crystal structure and has not been reported previously[25]. At 250 GPa, the bent H_3 units are linked to form spiral chains running along the c axis of the $R\bar{3}m$ structure (Fig. 1C). In SrH_8, the H_2 and H moieties have re-appeared at 50 and 150 GPa with space group $Cmc2_1$ and $P2_1/c$, respectively. At 50 GPa, SrH_{10} had a $P2_1/m$ structure again formed from H_2 and H. At 150 GPa, a $P2/c$ structure consisting of bent H_3 molecules was found to be the most stable. At 300 GPa, the $P2/c$ phase transformed to a $R\bar{3}m$ which is composed of graphene-like puckered hexagonal layers formed from atomic H (Fig. 1C).

From the description presented above, a general trend on the evolution of H-containing species with H concentration becomes apparent. At the lowest H concentration (*i.e.*, SrH_2), the H atoms were monatomic. In SrH_4, monatomic H and H_2 with the H–H distance of 0.790 Å became favourable. SrH_6 highlights the competition on the formation H_2 and H with H_3; in this case, the

H–H distance lengthened to 0.898 Å. On further compression, bent H_3 species start to appear and subsequently polymerized into spiral chains. In SrH_8 and SrH_{10}, the H_2 and H species re-appeared. At 50 GPa, both structures show H-H units with distances between 0.73–0.79 Å, that are close to that in free molecular H_2. The presence of H atoms as hydrides in SrH_2 is not surprising given an ionic structure is already observed under ambient conditions[37]. This can be rationalized straightforwardly from assuming a complete transfer of two valence electrons from Sr to the anti-bonding orbital of a molecular H_2 and breaks the molecule into two H^-. On a qualitative level, it is not unreasonable to expect structures of the H species presented in the high pressure solids at different stoichiometries are related to the available electrons donated by the Sr atoms.

The quantification of the electron transfer from the electropositive Sr to H_2 requires scrutiny. In Fig. 2, the iso-surface of the charge density difference ($\Delta\rho = \rho(SrH_{2n}) - [\rho(Sr\square_{2n}) + \rho(\square H_{2n})$; $\square$ indicates vacant Sr or H sites in the SrH_{2n} structure) for SrH_{2n} (n=1-5) at 150 GPa are compared. Significant electron transfer from Sr to the H species is indicated by charge depletion (blue) at the Sr site with concomitant charge accumulation (red surface) on the H species. In SrH_2, the accumulation of charge density is typical of hydride (H^-) atoms. For SrH_4 in the *Cmcm* structure, electrons from Sr are transferred to both the H atoms and H_2 molecules. Accordingly, the H-H bond length has elongated from the free molecule value of 0.742 Å to 0.816 Å. In view of the long closest H_2…H contact of 1.559 Å, the arrangement of the H atoms is obviously inconsistent with a hexagonal lattice suggested previously[25]. Only triangular H_3 units exist in the $P\bar{3}$ structure of SrH_6. The electrons are accumulated on the terminal H-atoms, as expected for the occupation of the non-bonding orbital of a H_3 species. In the $P2_1$ structure of SrH_8, the excess electron is localized on an isolated H atom which is 1.166 Å from a pair of H atoms with H-H distance of 0.797 Å, indicative of a loosely bound H^-…H_2 moiety. In SrH_{10}, both H_2 and H_3 units are presence with the transferred electrons occupying the nonbonding orbital of H_3. The H_3 unit has H-H distances of 0.96 Å and a valence ∠H-H-H angle of 149°. The H-H distance in the H_2 unit is 0.839 Å and the closet H_3…H_2 contact distance is 1.30 Å.

The charge transfers shown pictorially in Fig. 2 are quantified from the calculations of the atomic charges based on Bader's quantum theory of atom-in-molecule (QTAIM)[38, 39]. The calculated charges for the various H species in the SrH_{2n} (n=1,5) polymorphs at 150 GPa are summarized below (scheme **I**).

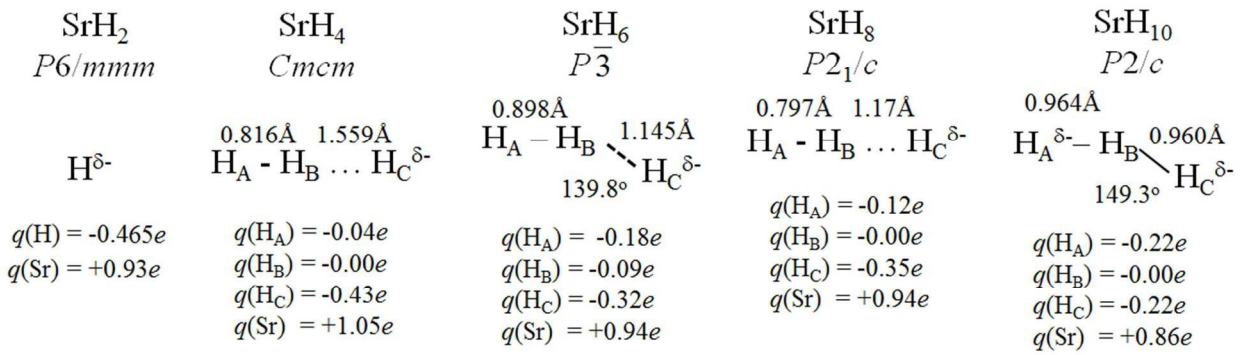

I

Bader charge analysis confirms the ionic character of the Sr atoms. Remarkably, among this series of compounds, the charge on Sr only spans a narrow range from +0.93*e* to +1.05*e*. These values are also comparable or even larger than the prototypical ionic NaCl solid where the Bader charge on the Na is +0.878*e*[40]. The charge on the hydridic hydrogen varied from -0.32*e* to -0.43*e*. In the H_3 unit of SrH_{10}, the charges are located on the two terminating H atoms each with -0.22*e*, as expected for the occupation of the non-bonding orbital.

Electronegativity is a fundamental chemical property that determines the affinity of an atom or a functional group to electrons. In the Mulliken scale[41] of electronegativity, χ, is defined as the arithmetic mean of the ionization potential and electron affinity. From density functional theory[42], the Mulliken electronegativity of molecular H_2 has been calculated to be 5.441 eV. The Mulliken electronegativity can then be converted to the more common Pauling scale with a recent formula[43] giving χ(Pauling) = 1.71 for a H_2 molecule. Remarkably, the Pauling electronegativity for molecular H_2 is close to group 13 and 14 elements with χ =1.61–2.33. Since the electronegativity of Sr is 0.95, the relatively large electronegativity difference (Δχ = 0.76) between Sr and H_2 would suggest polar bonding in the SrH_{2n} polymorphs. The ability of the H_2 in accepting the electrons in different high pressure crystalline phases helps to explain the existence of a variety of H species.

To illustrate our proposal, we consider the formation of SrH_4. Since formally two valence electrons are available from a single Sr atom, possible combinations of the products are $H_2 + 2H^-$ and $2H_2^-$. Intuitively, the first reaction will benefit from ionic interaction between the hydrides and the Sr^{2+} cations and more efficient packing of H^- anions at high pressure. Indeed, the theoretically predicted stable structures of SrH_4 at 50 and 150 GPa indeed shows the presence of

monatomic H and molecular H_2 with a bond length of *ca*. 0.79 Å, which is comparable to the isolated molecule. The structural motifs of SrH_8 and SrH_{10} at 50 GPa can be interpreted in a similar manner. In each case, a maximum of two electrons can be accepted by the H_2, and the resulting products are $3H_2 + 2H^-$ and $4H_2 + 2H^-$, respectively, which are also consistent with the predicted structural motifs. At 50 GPa, the H–H separations in the H_2 moieties of the two crystals are almost similar (0.77 Å). Note that the shortest $Sr^{2+}\cdots H^-$ contacts in SrH_4, SrH_6, SrH_8, and SrH_{10} at 50 GPa are all within 1.87–1.93 Å and are not sensitive to the crystal structures.

A unique case is SrH_6. At 50 and 150 GPa, the stable structures are composed of $H_2 + H^-$ moieties. Further compression of SrH_6 reveals two new structures at 200 and 250 GPa. At 200 GPa, a structure of bent H_3 molecules with a *P*321 space group emerged. The formation of the bending H_3 requires the participation of H orbitals of *p* symmetry (scheme **II**). This was confirmed by the calculated integrated projected density of states (Fig. 3), which clearly shows a gradual increase and widening of the H *p*-valence band of SrH_6 with increasing pressure. The number of *p* electrons has nearly doubled (from 0.22*e* / state to 0.4*e* / state) as the pressure is increased from 100 to 300 GPa. At higher pressure, the bent H_3 units are compressed closer together and begin to interact in the crystal structure. The orbital correlation diagram (Fig. 4) at the zone center (Γ) shows overlap of the filled highest occupied crystal orbital with an empty anti-bonding orbital at Γ. Consequently, polymeric chains spiral down the threefold screw axis along the *c*-direction of the $R\bar{3}m$ structure is observed at 250 GPa. Similar chain structure was also observed in the high-pressure phase IV of sulphur (S-IV)[44]. In fact the spiraling H-chains in SrH_6 and S-IV share many geometrical similarities. Phonon calculations showed that the successive $P\bar{3} \rightarrow P321 \rightarrow R\bar{3}m$ transitions are driven by soft phonons and are likely second order in nature[45] (see supplementary materials). The calculated enthalpies show that the $P\bar{3}$ and *P*321 structures are very close in the pressure range 150–200 GPa and that they become almost degenerate with the $R\bar{3}m$ structure at above 250 GPa.

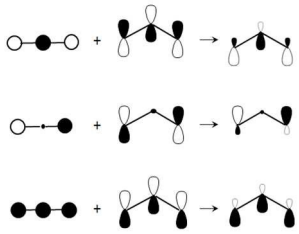

II

The description for the structural evolution of the high pressure strontium hydride polymorphs presented here is different from the explanation offered the earlier study[25]. Previously, it was argued that the gradual development of hexagonal layers of H atoms forms the primary building block for the high pressure structures. In some cases, in order to satisfy this condition, unphysical linkage with very long H…H distances (> 1.5 Å) was invoked. To illustrate this point, in Fig. 5 we plotted the H networks in *Cmcm*-SrH_4 and $P\bar{3}$-SrH_6 at 150 GPa using two linkage cutoff criteria *viz*. 1.15 Å and 1.55 Å. As shown in the charge density difference analysis (*vide infra*), a H…H separation < 1.15 Å is an acceptable distance for weak interaction between H_2 and $H^{\delta-}$; whilst 1.55 Å is too far for any reasonable interaction. It is clear from Fig. 5 that unless an unrealistically large distance criterion is used there is no evidence of hexagonal layers in SrH_4, a proposed precursor for forming the cage structure analogues to CaH_6 in SrH_6.

The *P*2/c structure of SrH_{10} contains H_2 and H_3 units that are stable up to 300 GPa. At higher pressure, it transformed into a $R\bar{3}m$ structure with Sr atoms sandwiched between double staggered puckered graphene-like H-layers. The H-H distances of the hexagonal layer alternate between 0.998 and 1.011 Å and the out of plane ∠H-H-H angle 153.8° (180° for a perfect plane). Similar graphene like layer has also been proposed recently in the high pressure phase-IV stable above 270 GPa of solid hydrogen[36]. The presence of similar hexagonal atomic layers in SrH_{10} is significant as this serves as another proof of a suggestion that a charge-transfer from the molecule-like "Br_2" H_2 layers in phase-IV of solid hydrogen[46] is important to the formation of the "graphene-like" layers.

The chemical behaviour of H^- is often compared to the iodide (I^-) anion. To the best of our knowledge, there have been no theoretical or experimental investigations on the metal-iodide system. However, in a recent study on the sodium chlorides ($NaCl_n$), linear but asymmetric Cl_3^- units was predicted and confirmed in $NaCl_3$[47]. Furthermore, at higher Cl concentration as in $NaCl_7$, the most stable structure was predicted to have a self-clathrate framework with Cl atoms located at the centers of the cavities. The transformation from linear Cl_3^- to the polyhedra structure in the sodium chlorides is similar to the structural evolution found in CaH_n[24]. It is desirable to extend similar structural search to MI_n systems (M: group II elements) at high pressure to further investigate if there is any connection between the structures metal hydrides and iodides at high pressure. In passing, it is noteworthy that the structures and chemical bonding of high pressure solid hydrogen have been discussed in detail recently[48-51].

Conclusion

In summary, the phase stabilities and structures of SrH_{2n} (n = 1–5) in the pressure range 50–300 GPa were systematically investigated using CALYPSO method and two likely candidates for the high-pressure phases of SrH_6 (*P*321) and SrH_{10} (*R*-3*m*) were firstly uncovered at 200 and 300 GPa, respectively. Structural analysis of the predicted stable high-pressure polymorphs of SrH_{2n} (n = 1–5), *via* assumed reactions of Sr with H_2, was able to explain the occurrence on a variety of H structural units (motifs). Our calculations indicate that the existence of various H species of high-pressure polymorphs of SrH_{2n} can be ascribed to the charge transfers from Sr to the hydrogen. This rather simplistic description may serve as a guide to predict and rationalize the complexity of H-species in the high-pressure polymorphs of SrH_{2n} and can be extended to aid the interpretation of the structures of other binary metal alloys at high pressure.

Acknowledgements

Y. W, H. W, J. T and Y. M are thankful to the financial support by Natural Science Foundation of China (NSFC) under 11474128, 11274136, 11474126 and 11404128, the China 973 Program (2011CB808200), China Postdoctoral Science Foundation (No. 2014M551181), the 2012 One Thousand Talents Scheme, the 2012 Changjiang Scholars Program of China and Changjiang Scholar and Innovative Research Team in University (IRT1132). T. I. was supported by Ministry of Education, Culture, Sports, Science and Technology of Japan (20103001–20103005). The calculations were performed in the computing facilities at Rikagaku Kenkyūjo Integrated Cluster of Clusters system (Japan) and the High Performance Computing Center of Jilin University.

References

1. W. Grochala, R. Hoffmann, J. Feng and N. W. Ashcroft, *Angew. Chem. Int., ed. Engl.*, 2007, **46**, 3620-3642.
2. J. S. Tse, *Z. Krist.*, 2005, **220**, 521-530.
3. M. McMahon, R. Nelmes and S. Rekhi, *Phys. Rev. Lett.*, 2001, **87**, 255502.
4. C. L. Guillaume, E. Gregoryanz, O. Degtyareva, M. I. McMahon, M. Hanfland, S. Evans, M. Guthrie, S. V. Sinogeikin and H. Mao, *Nat. Phys.*, 2011, **7**, 211-214.
5. M. McMahon, E. Gregoryanz, L. Lundegaard, I. Loa, C. Guillaume, R. Nelmes, A. Kleppe, M. Amboage, H. Wilhelm and A. Jephcoat, *Proc. Natl. Acad. Sci. U S A.*, 2007, **104**, 17297-17299.
6. T. Matsuoka and K. Shimizu, *Nature*, 2009, **458**, 186-189.
7. Y. Ma, M. Eremets, A. R. Oganov, Y. Xie, I. Trojan, S. Medvedev, A. O. Lyakhov, M. Valle and V. Prakapenka, *Nature*, 2009, **458**, 182-185.
8. V. Heine, *Nature*, 2000, **403**, 836-837.
9. E. Wigner, *Phys. Rev.*, 1934, **46**, 1002.
10. Y. Yao, S. T. John, Z. Song and D. D. Klug, *Phys. Rev. B*, 2009, **79**, 092103.
11. R. Sternheimer, *Phys. Rev.*, 1950, **78**, 235.

12. T. Atou, M. Hasegawa, L. Parker and J. Badding, *J. Am. Chem. Soc.*, 1996, **118**, 12104-12108.
13. N. Ashcroft, *Phys. Rev. Lett.*, 2004, **92**, 187002.
14. A. Drozdov, M. Eremets and I. Troyan, *arXiv preprint arXiv:1412.0460*, 2014.
15. A. R. Oganov and C. W. Glass, *J. Chem. Phys.*, 2006, **124**, 244704.
16. Y. Wang, J. Lv, L. Zhu and Y. Ma, *Phys. Rev. B*, 2010, **82**, 094116.
17. C. J. Pickard and R. Needs, *Phys. Rev. Lett.*, 2006, **97**, 045504.
18. Y. Wang and Y. Ma, *J. Chem. Phys.*, 2014, **140**, 040901.
19. J. Hooper and E. Zurek, *Chem. Plus. Chem*, 2012, **77**, 969-972.
20. J. Hooper and E. Zurek, *J. Phys. Chem. C*, 2012, **116**, 13322-13328.
21. J. Hooper and E. Zurek, *Chemistry-A European Journal*, 2012, **18**, 5013-5021.
22. A. Shamp, J. Hooper and E. Zurek, *Inorg. Chem.*, 2012, **51**, 9333-9342.
23. D. C. Lonie, J. Hooper, B. Altintas and E. Zurek, *Phys. Rev. B*, 2013, **87**, 054107.
24. H. Wang, S. T. John, K. Tanaka, T. Iitaka and Y. Ma, *Proc. Natl. Acad. Sci. U S A.*, 2012, **109**, 6463-6466.
25. J. Hooper, T. Terpstra, A. Shamp and E. Zurek, *J. Phys. Chem. C*, 2014, **118**, 6433-6447.
26. J. Hooper, B. Altintas, A. Shamp and E. Zurek, *J. Phys. Chem. C*, 2013, **117**, 2982-2992.
27. Y. Wang, J. Lv, L. Zhu and Y. Ma, *Comp. Phys. Comm.*, 2012, **183**, 2063-2070.
28. J. P. Perdew, K. Burke and M. Ernzerhof, *Phys. Rev. Lett.*, 1996, **77**, 3865.
29. G. Kresse and J. Furthmüller, *Comput. Mater. Sci.*, 1996, **6**, 15-50.
30. P. E. Blöchl, *Phys. Rev. B*, 1994, **50**, 17953.
31. H. J. Monkhorst and J. D. Pack, *Phys. Rev. B*, 1976, **13**, 5188.
32. K. Parlinski, Z. Li and Y. Kawazoe, *Phys. Rev. Lett.*, 1997, **78**, 4063.
33. A. Togo, F. Oba and I. Tanaka, *Phys. Rev. B*, 2008, **78**, 134106.
34. K. Momma and F. Izumi, *J. Appl. Crystallogr.*, 2011, **44**, 1272-1276.
35. M. Eremets and I. Troyan, *Nat. Mater.*, 2011, **10**, 927-931.
36. R. T. Howie, C. L. Guillaume, T. Scheler, A. F. Goncharov and E. Gregoryanz, *Phys. Rev. Lett.*, 2012, **108**, 125501.
37. S. D. J.S. Smith, D.D. Klug and J.S. Tse, *Solid. Stat. Commun.*, 2009, **179**.
38. F. Richard and R. Bader, Oxford University Press, Oxford, 1990.
39. G. Henkelman, A. Arnaldsson and H. Jónsson, *Comput. Mater. Sci.*, 2006, **36**, 354-360.
40. M. Yu and D. R. Trinkle, *J. Chem. Phys.*, 2011, **134**, 064111.
41. R. S. Mulliken, *J. Chem. Phys.*, 1934, **2**, 782-793.
42. C.-G. Zhan, J. A. Nichols and D. A. Dixon, *J. Phys. Chem. A*, 2003, **107**, 4184-4195.
43. D. R. Herrick, *J. Chem. Theory Comput.*, 2005, **1**, 255-260.
44. L. Crapanzano, W. A. Crichton, G. Monaco, R. Bellissent and M. Mezouar, *Nat. Mater.*, 2005, **4**, 550-552.
45. H. E. Stanley, *Introduction to Phase Transitions and Critical Phenomena, by H Eugene Stanley, pp. 336. Foreword by H Eugene Stanley. Oxford University Press, Jul 1987. ISBN-10: 0195053168. ISBN-13: 9780195053166*, 1987, **1**.
46. A. F. Goncharov, S. T. John, H. Wang, J. Yang, V. V. Struzhkin, R. T. Howie and E. Gregoryanz, *Phys. Rev. B*, 2013, **87**, 024101.
47. W. Zhang, A. R. Oganov, A. F. Goncharov, Q. Zhu, S. E. Boulfelfel, A. O. Lyakhov, E. Stavrou, M. Somayazulu, V. B. Prakapenka and Z. Konôpková, *Science*, 2013, **342**, 1502-1505.
48. V. Labet, P. Gonzalez-Morelos, R. Hoffmann and N. Ashcroft, *J. Chem. Phys.*, 2012, **136**, 074501.
49. V. Labet, R. Hoffmann and N. Ashcroft, *J. Chem. Phys.*, 2012, **136**, 074502.
50. V. Labet, R. Hoffmann and N. Ashcroft, *J. Chem. Phys.*, 2012, **136**, 074503.
51. V. Labet, R. Hoffmann and N. Ashcroft, *J. Chem. Phys.*, 2012, **136**, 074504.

Fig. 1 (A) Enthalpies of formation (ΔH, with respect to SrH_2 and solid H_2) of SrH_x at pressures of 50, 150, and 300 GPa. The abscissa x is the fraction of H_2 in the structures. Circles show the metastable structures. (B) The phase transition sequences of strontium polyhydrides and the reference phases at pressures of 50 to 330 GPa. (C) The predicted lowest-enthalpy structures stable relative to SrH_2 and a 1×1×2 supercell of $R\bar{3}m$-SrH_6 is shown to represent the $(H_3^-)_\infty$ spiral chain, for which only a fragment is given in the label.

Fig. 2 The iso-surface of the charge density difference for SrH_2 (*P*6/*mmm*), SrH_4 (*Cmcm*), SrH_6 ($P\bar{3}$), SrH_8 ($P2_1/c$) and SrH_{10} (*P*2/*c*) at 150 GPa with charge density of ±0.09 e/Å^3. The charge depletion and accumulation are shown in blue and red, respectively.

Fig. 3 (a) Integrated PDOS of H *p* orbitals of SrH_6 at pressures up to 300 GPa. (b) PDOS of H atom of *P*321-SrH_6 at 150 GPa. The vertical dotted lines indicate the Fermi level.

Fig. 4 Orbital correlation diagram for H_3 fragments at the zone center (Γ) in the $R\bar{3}m$ structure of SrH_6.

Fig. 5 The H networks in *Cmcm* SrH_4 and $P\bar{3}$-SrH_6 at 150 GPa.

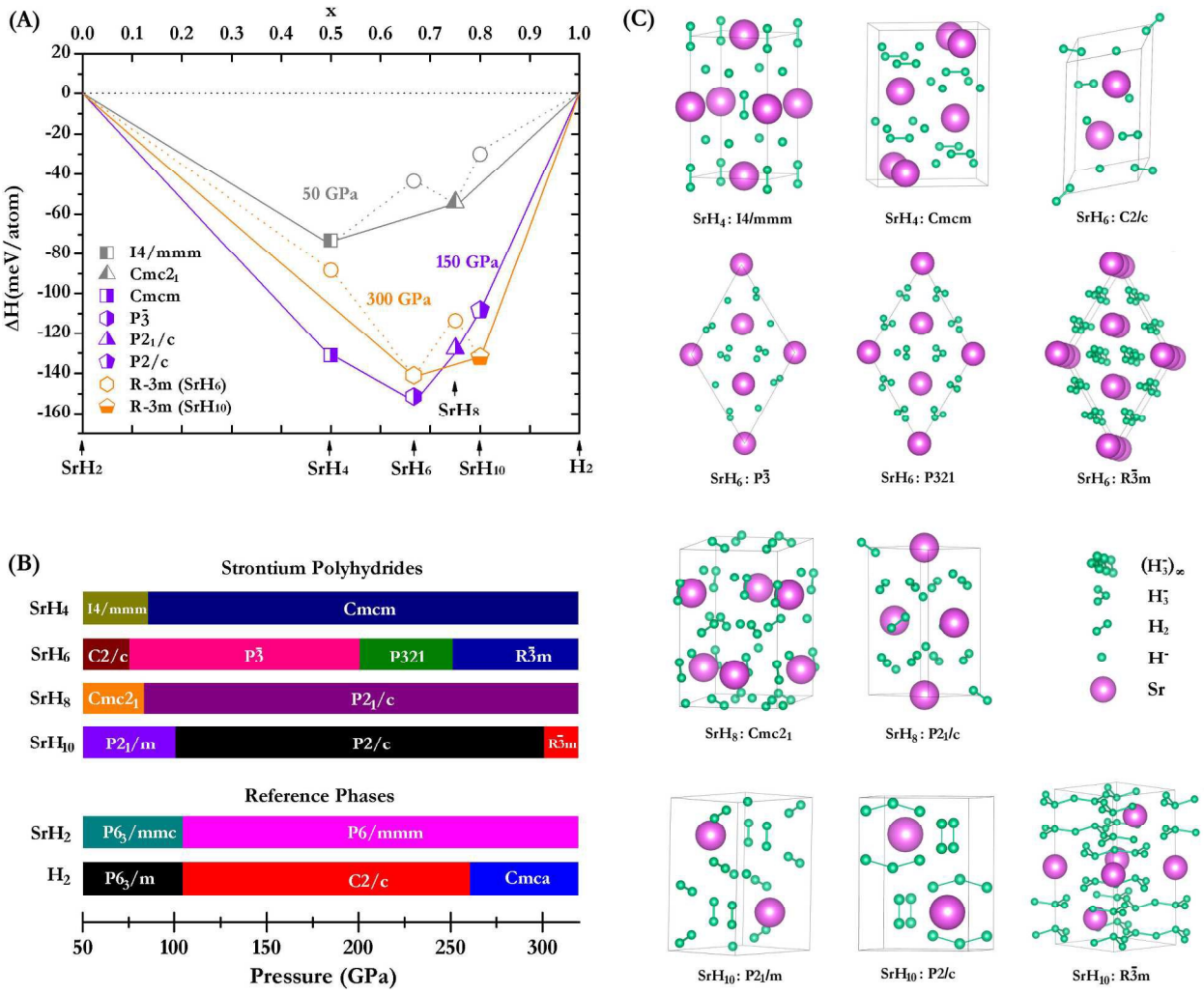

Fig. 1

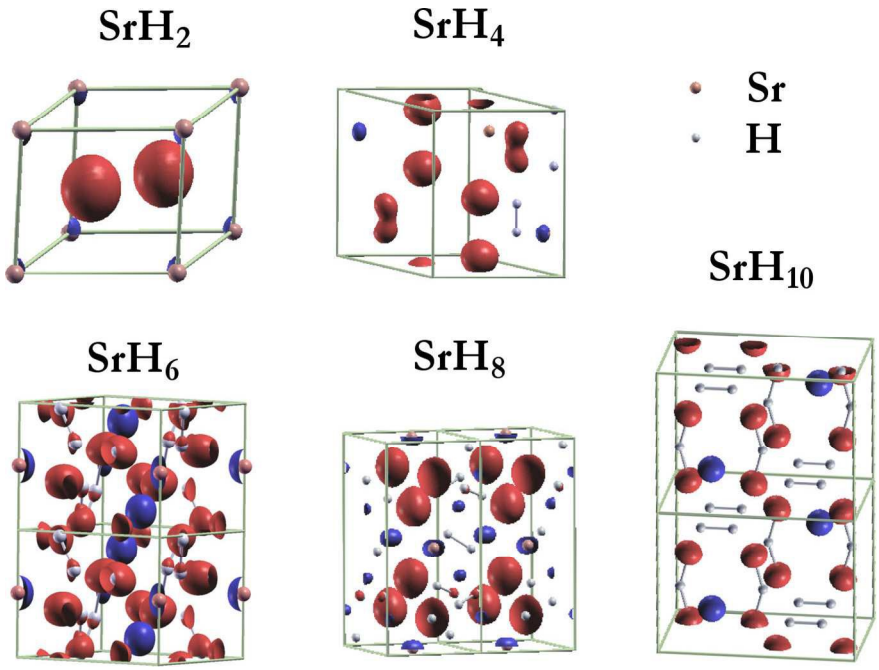

Fig. 2

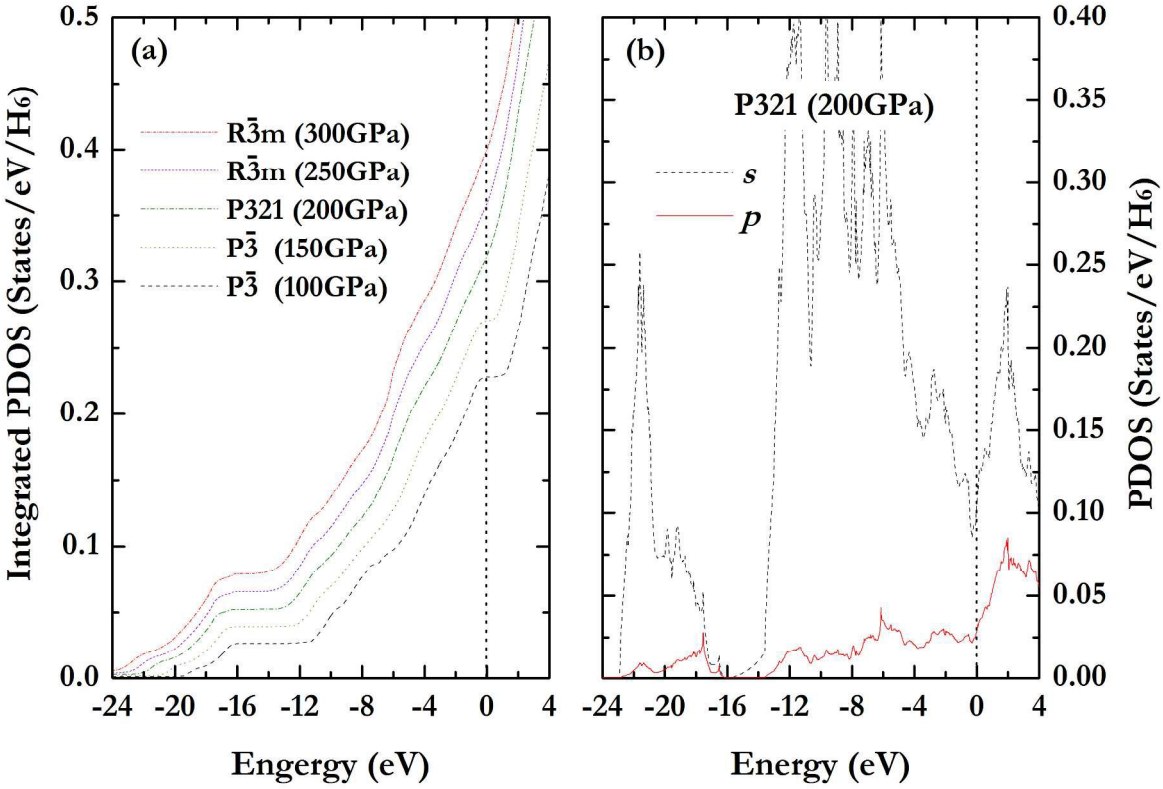

Fig. 3

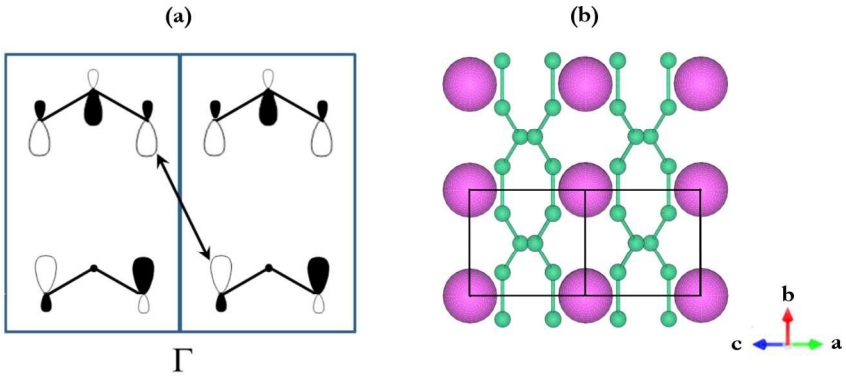

Fig. 4

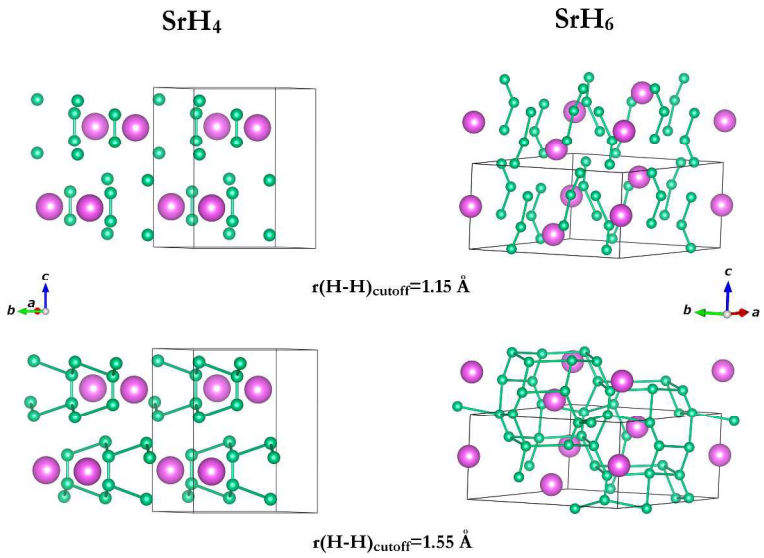

Fig. 5